Eur. Phys. J. C (2025) 85:973
https://doi.org/10.1140/epjc/s10052-025-14666-0

THE EUROPEAN PHYSICAL JOURNAL C

Regular Article - Theoretical Physics

Influence of quantum correction on Kerr black hole in effective loop quantum gravity via shadows and EHT results

Muhammad Ali Raza[1,a], **M. Zubair**[1,2,b], **Farruh Atamurotov**[3,4,5,c], **Ahmadjon Abdujabbarov**[6,7,d]

[1] Department of Mathematics, COMSATS University Islamabad, Lahore Campus, Lahore, Pakistan
[2] National Astronomical Observatories, Chinese Academy of Sciences, Beijing 100101, China
[3] Kimyo International University in Tashkent, Shota Rustaveli str. 156, 100121 Tashkent, Uzbekistan
[4] University of Tashkent for Applied Sciences, Str. Gavhar 1, 100149 Tashkent, Uzbekistan
[5] Research Center of Astrophysics and Cosmology, Khazar University, 41 Mehseti Street, 1096 Baku, Azerbaijan
[6] New Uzbekistan University, Movarounnahr Street 1, 100000 Tashkent, Uzbekistan
[7] School of Physics, Harbin Institute of Technology, Harbin 150001, People's Republic of China

Received: 30 March 2025 / Accepted: 23 August 2025

Abstract Recently, a study on shadow of quantum corrected Schwarzschild black hole in loop quantum gravity appeared in (Ye et al. in Phys Lett B 851:138566, 2024, https://doi.org/10.1016/j.physletb.2024.138566) assuming a fixed value of Barbero–Immirzi parameter γ. Following this approach, we considered its rotating counterpart being a quantum corrected Kerr black hole in effective loop quantum gravity and studied its deviation from Kerr black hole for a fixed value of γ. We proposed and proved a theorem describing the location of unstable circular null orbits for all such Kerr-like metrics. The deviation between the shadows of the Kerr and quantum corrected Kerr black holes has also been studied, and the spin parameter is constrained by comparison with the EHT results for M87* and Sgr A* to precisely probe the quantity of deviation due to quantum correction. Lastly, we immersed the quantum corrected Kerr black hole in an inhomogeneous plasma and studied its impact on the shadow size. We found that the unstable null orbits for the quantum corrected Kerr black hole are always smaller than the unstable null orbits for Kerr black hole. The effect of Barbero–Immirzi parameter allows the quantum corrected Kerr black hole to mimic Sgr A* with a higher probability than the Kerr black hole. However, the quantum corrected Kerr black hole does not mimic M87*. The plasma reduces the size of the shadow of quantum corrected black hole, and the plasma parameter in the case II is more sensitive than that in case I.

1 Introduction

Soon after the foundation of General Relativity, Schwarzschild [1] proposed a black hole metric as the pioneering solution of Einstein field equations in vacuum. However, this black hole metric encompasses a spacetime singularity, a region where all physical laws breakdown and nothing can be explained [2]. Though, in classical regime, General Relativity is a well understood theory and may explain various phenomena in gravitational physics. However, it has failed to resolve the singularity problem. Penrose [3] proposed that the spacetime singularity is inevitable, and later, Hawking and Penrose [4] proposed the inevitability of the singularity in Big Bang.

To resolve the singularity issue, various attempts have been made over the years and thus one may expect a quantum theory of gravity may resolve the issue. One of the proposed theories for quantum gravity is loop quantum gravity (LQG), characterized by its independence from a fixed background and its non-perturbative approach [5–9]. The theoretical and numerical aspects of Loop Quantum Cosmology (LQC) have provided solutions to the cosmological big-bang singularity [10–14]. Some approaches to resolve the singularity of the Schwarzschild black hole involve quantization of its interior using techniques derived from LQG [15–22]. Moreover, studies have explored the LQG corrections related to black hole formation and gravitational collapse in different theoretical models [23–27].

[a] e-mail: maliraza01234@gmail.com
[b] e-mails: mzubairkk@gmail.com; drmzubair@cuilahore.edu.pk (corresponding author)
[c] e-mail: atamurotov@yahoo.com
[d] e-mail: ahmadjon@astrin.uz

Published online: 11 September 2025

Recently, Lewandowski et al. [28] investigated gravitational collapse of a dust ball by incorporating quantum effects from LQG, using a LQC framework. They found that the collapse halts when the dust ball's energy density reaches the Planck scale, causing the dust to bounce instead of continuing to collapse. By matching the metrics at the boundary between the collapsing dust ball's interior and exterior, they derived a quantum corrected Schwarzschild metric for the external spacetime. This work highlights how quantum gravity influences the behavior of collapsing structures. Later, Ye et al. [29] studied the shadow and photon rings of this quantum corrected black hole. He found that this quantum corrected black hole can be distinguished from the Schwarzschild black hole in terms of shadow images in some illumination models. They assumed the fixed value of the Barbero–Immirzi parameter and hence the parameter α was not treated as a free parameter. Their findings were presented in comparison with the results of Schwarzschild black hole. Motivated by this, assuming the fixed value of the Barbero–Immirzi parameter, we will accomplish our analysis in comparison with the results of Kerr black hole for the rotating case.

In 2000, Falcke et al. [30] predicted the possibility of imaging black holes especially Sgr A*, which got verified by the discovery of images of the supermassive black hole M87* [31,32] and Sgr A* [33,34] by the Event Horizon Telescope (EHT) that has opened up new avenues in black hole physics. These images comprise light rings and shadows of black holes with nearly equal radii. A light ring is formed by the trapping of light and appears as a glowing image of radius greater than the event horizon. Whereas, the shadow is not a physical entity, but a dark 2D silhouette formed by the disappearing of photons from the sight of an observer at infinity. Since then, many studies have been accomplished to understand the shape and size of the black hole shadow in various different models and frameworks, see Refs. [35–48]. The images of M87* and Sgr A* provided the data which has been useful in testing various gravity theories by determining constraints on the parameters associated with the theories, see Refs. [49–66]. In particular, Islam et al. [53] investigated LQG by using the EHT data for M87* and Sgr A*. They considered a rotating polymerized black holes in LQG which acts as Kerr black hole asymptotically. Using the shadow analysis, the LQG parameter has been constrained and found that a significant part of parametric spaces for one and two horizon black holes is consistent with the EHT results for both M87* and Sgr A*. Moreover, the EHT results for Sgr A* also agree with the triple horizon black hole, but not for the M87*. Afrin et al. [54] investigated the LQG for the results of M87* and Sgr A* by considering two rotating LQG-inspired black holes and found that the upper bound for LQG parameter obtained from the results of Sgr A* is more precise than the upper bound from M87*. The astrophysical black holes are surrounded by plasma due to a huge gravity and in-falling matter [67]. This may certainly last an impact on the light propagation causing deviation in shadows. The study of light propagation in magnetized plasma with no pressure, is governed by the Hamiltonian derived by Breuer and Ehlers [68,69]. Later, Perlick and Tsupko [70] derived the Hamiltonian formulation for a rather simpler case of a plasma without pressure and magnetization. Perlick et al. [71] also explored the shadow of static and spherically symmetric black holes immersed in a plasma medium. Recently, various black hole solutions have been considered to investigate their shadows in the presence of plasma, see Refs. [58,72–77].

Inspired by [29], we consider the recently developed rotating counterpart [78–80] of the quantum corrected Schwarzschild black hole [28], since the supermassive black holes are rotating in nature. Our major goal is to test the LQG effects under the influence of Barbero–Immirzi parameter, by comparing its shadow results with the EHT data and for Kerr black hole. In particular, we investigate the deviation of the quantum corrected Kerr black hole from the Kerr black hole via EHT results. We also study the impact of plasma on the shadow of quantum corrected Kerr black hole. The paper is organized as: In Sect. 2, we present a brief overview of the static and rotating black hole metrics, and further discuss its horizon structure in terms of black hole spin. In Sect. 3, we employ the dynamical methods for the null geodesics, and effective potential and shadows are studied in comparison with result of Kerr black hole. The Sect. 4 comprises the constraints on the spin of black hole parameters in comparison with EHT data. In Sect. 5, we investigate the impact of plasma on shadows. Lastly, in Sect. 6, we present a brief conclusion and future prospects. Note that, we consider $G = \hbar = c = 1$ in our calculations, unless otherwise mentioned.

2 The static and rotating quantum corrected black hole metrics

In this section, we review the basic concepts and the development of the quantum corrected Schwarzschild black hole metric and its rotating counterpart. The Oppenheimer–Snyder model [81] describes the collapse of dust matter. Since, the model describes the Big Bang singularity, therefore, it was proposed to consider a Big Bounce instead of the Big Bang [82]. It is also proposed that quantum gravity can resolve the singularity problem, therefore, a Big Bounce is also supported by LQC [12,83,84]. A 4D spherically symmetric Ashtekar–Pawlowski–Singh (APS) metric [12] given as

$$\mathrm{d}s^2_{\mathrm{APS}} = -\mathrm{d}\tau^2 + a(\tau)^2\mathrm{d}\tilde{r}^2 + a(\tau)^2\tilde{r}^2\mathrm{d}\Omega_2^2, \tag{1}$$

where, $\mathrm{d}\Omega_2^2 = \mathrm{d}\theta^2 + \sin^2\theta\mathrm{d}\phi^2$ is the metric of a 2-sphere and $a(\tau)$ satisfies a deformed Friedmann equation in terms

of Hubble parameter $\tilde{H}$ given as

$$\tilde{H}^2 := \left(\frac{\dot{a}}{a}\right)^2 = \frac{8\pi G\rho}{3}\left(1-\frac{\rho}{\rho_c}\right), \tag{2}$$

such that the energy density of the collapsing dust ball is given as $\rho = 3M/\left(4\pi\tilde{r}_0^3 a^3\right)$. The dot in Eq. (2) denotes the differentiation with respect to the proper time τ. Moreover, the critical energy density ρ_c causes the deformation with a constant value equal to $\sqrt{3}/\left(32\pi^2\gamma^3 G^2\hbar\right)$. Note that M is the mass of the dust ball with radius $a(\tau)\tilde{r}_0$, γ is the Barbero–Immirzi parameter of LQG [85,86], whereas, G and $\hbar$ are Newton's and Planck's constants, respectively. The mass of the dust ball does not vary due to the conservation of the energy-momentum tensor. The classical regime corresponds to $\rho \ll \rho_c$, whereas, the energy density of the ball is never infinite for which the APS metric does not exhibit any singularity. Any particle inside the dust ball satisfies the inequality $0 \leq \tilde{r} \leq \tilde{r}_0$.

The quantum Oppenheimer–Snyder (qOS) model is given by the metric

$$\mathrm{d}s^2_{\mathrm{qOS}} = -\left(1-F(r)\right)\mathrm{d}t^2 + \frac{\mathrm{d}r^2}{1-H(r)} + r^2\mathrm{d}\Omega_2^2. \tag{3}$$

The interior region is described by the APS metric as a dust ball, and the exterior one is depicted by vacuum qOS metric. The θ and ϕ coordinates are same for both metrics, whereas, the coordinates τ and $\tilde{r}$ in the ball are matched on to the coordinates t and r in the exterior region. The dust interface $\tilde{r} = \tilde{r}_0$ is important region in APS spacetime, with coordinates $(t(\tau), r(\tau), \theta, \phi)$ in the other spacetime. Using the Israel junction conditions, which require continuity of the metrics and extrinsic curvature on the interface between dust and vacuum, the coordinates are matched as $(\tau, \tilde{r}_0, \theta, \phi) \sim (t(\tau), r(\tau), \theta, \phi)$, generating a quantum-corrected Schwarzschild metric in LQG given by [28]

$$\begin{aligned}\mathrm{d}s^2_{\mathrm{qOS}} = &-\left(1-\frac{2M}{r}+\frac{\alpha M^2}{r^4}\right)\mathrm{d}t^2 \\ &+\left(1-\frac{2M}{r}+\frac{\alpha M^2}{r^4}\right)^{-1}\mathrm{d}r^2 + r^2\mathrm{d}\Omega_2^2,\end{aligned} \tag{4}$$

where, the quantum correction parameter $\alpha = 16\sqrt{3}\pi\gamma^3 l_p^2$ causes the deformation in the Schwarzschild metric, and $l_p = \sqrt{G\hbar}$ defines the Planck length. It is understood that the Barbero–Immirzi parameter has a fixed value $\gamma \approx 0.2375$ [85,86] that gives a fixed value of the parameter $\alpha \approx 1.1663$ under the assumption $\hbar = G = 1 = c$ in natural units.

At the interface, the radius of the dust ball being $a(\tau)\tilde{r}_0$ is equal to the radius $r(\tau)$ in the other spacetime, therefore, taking the derivative on both sides and then squaring gives the value of $H(r(\tau))$, (for complete derivation, see Appendix A in Ref. [28]). Along the radial geodesic, when $\dot{r} = 0$, we have $H(r) = 0$ which gives the lower bound of the radial coordinate, that is,

$$r_b = \left(\frac{\alpha M}{2}\right)^{\frac{1}{3}}. \tag{5}$$

This implies that the radius of the dust surface $a(\tau)\tilde{r}_0 \in [r_b, \infty)$ and thus $r \geq r_b$. The mass M of the dust ball is now the mass of the quantum-corrected black hole that has a minimum value $M_{\min} = \frac{16\gamma\sqrt{\pi\gamma}}{3\sqrt[4]{3}}$. Below this minimum value of M, there exists no horizon; however, there exist two horizons for $M > M_{\min}$ given as

$$r_\pm = \frac{\zeta\left(1\pm\sqrt{2\zeta-1}\right)\sqrt{\alpha}}{\sqrt{(1+\zeta)(1-\zeta)^3}}, \tag{6}$$

where, $\zeta \in (1/2, 1)$ is arbitrary parameter such that $4\alpha\zeta^4 = M^2\left(1-\zeta^2\right)^3$.

Recently, in Refs. [79,80,87,88], the authors have not considered the above-mentioned fixed value of the Barbero–Immirzi parameter, but accomplished their analyses by incorporating the variation of α. It is now well understood that γ has a fixed value, therefore, the minimum mass $M_{\min}$ and the deformation parameter α also have fixed values. Therefore, only M is the free parameter in the black hole metric (4). The extra term with α describes only the deviation in the quantum regime from the Schwarzschild metric depending on M. Generally, for each particular value of M, the deviation between the quantum corrected black hole and the Schwarzschild black hole is fixed due to the fact that α has a fixed value and cannot be varied around its prescribed value. Therefore, the studies mentioned above with variable α do not account for rigorous and feasible analyses.

The significance of studying rotating black holes can be highlighted through a comparison of their shadows with the EHT data on supermassive black holes as they are predominantly rotating in nature. Thus, considering rotating black holes allow us to establish a more accurate and rigorous analysis. The rotating counterpart of the metric (4) with effective geometry was derived in Refs. [78–80] so that the quantum corrected Kerr black hole in effective LQG in Boyer–Lindquist coordinates reads

$$\begin{aligned}\mathrm{d}s^2_{\mathrm{eff}} = &-\frac{\Delta(r)-a^2\sin^2\theta}{\rho^2}\mathrm{d}t^2 + \frac{\rho^2}{\Delta(r)}\mathrm{d}r^2 + \rho^2\mathrm{d}\theta^2 \\ &+\frac{\left(r^2+a^2\right)^2\sin^2\theta - \Delta(r)a^2\sin^4\theta}{\rho^2}\mathrm{d}\phi^2 \\ &-\frac{2a\sin^2\theta\left(a^2+r^2-\Delta(r)\right)}{\rho^2}\mathrm{d}t\mathrm{d}\phi,\end{aligned} \tag{7}$$

where,

$$\Delta(r) = r^2 + a^2 - 2Mr + \frac{\alpha M^2}{r^2}, \tag{8}$$

$$\rho^2 = r^2 + a^2\cos^2\theta, \tag{9}$$

where, a is the spin parameter. Since, the prescribed value of γ yields, $M_{\min} \approx 0.8314 < M$ is a valid limit for the black hole mass, therefore, we consider $M = 1$ throughout this work to focus on influence of a within the LQG regime.

For the static metric (4), it is now well understood that the covariance is modified and therefore is not classical anymore. Therefore, for the time-like diffeomorphisms, in general, a coordinate transformation that involves also the t coordinate, transforms the metric as in such a way that the tensors do not transform classically. However, it is not proved anywhere that this leads to inconsistent physics, even if by the other side also the opposite has not been proved. One should be capable, in principle, to construct scalars that are invariant under the new symmetry group, and derive consistent (modified) gauge invariant physics, but also this has not been done yet. Due to which it remains an open question. The underlying spherically symmetric model has classical covariance for the spatial diffeomorphisms as proved in the Refs. [89,90], whereas, the model does not exhibit covariance under time-like diffeomorphisms. In the Refs. [91,92], it has been proved that the model in the dust-time gauge is equivalent to a classically covariant mimetic model with the same gauge fixing. This does not imply that the effective model is classically covariant, but that the two are identical only in the dust-time gauge. Therefore, if one starts with the covariant mimetic model, gets the same result for the effective one in the dust-time gauge, and by the other side has classical covariance.

Since, the covariance is modified in static case for the spherical symmetry, the rotating metric may not be exact line element for its static counterpart giving rise to an effective geometry. For this reason, the metric (7) serves as an effective metric and therefore describes a quantum corrected Kerr black hole in effective LQG which encompasses the most probable properties of the exact rotating metric. For instance, the metric (7) reduces to the metric (4) when $a = 0$. By removing the quantum effects, the metric (7) reduces to the Kerr metric, just as the metric (4) reduces to Schwarzschild one. Moreover, the metric function $\Delta(r)$ can be written as

$$\Delta(r) = \Delta_{\text{Kerr}}(r) + \frac{\alpha M^2}{r^2}, \tag{10}$$

which shows that the metric (7) is a quantum corrected Kerr black hole metric with an additional term comprising LQG parameter. We have mentioned that the parameter α has a fixed value and we consider $M = 1$, thus, the only free parameter for the rotating metric is the spin a. Hence, we can rigorously analyze the deviation of quantum corrected Kerr black hole from the Kerr black hole. Like the Kerr metric, the quantum corrected Kerr metric also exhibits the time-translational and rotational invariance isometries corresponding to the Killing vector fields $(\partial_t)^\mu$ and $\left(\partial_\phi\right)^\mu$.

The last term in Eq. (10) has no dependence on a, therefore, the horizon curve will be unique with a certain deviation from the horizon curve of Kerr black hole. It is generated numerically by solving the equation $\Delta(r) = 0$ for real and positive roots. A clear deviation in two curves is shown in Fig. 1 in terms of horizon radii r_{h} with respect to a. It can be seen that the event horizon of the quantum corrected Kerr black hole is smaller than the event horizon of Kerr black hole. While the Cauchy horizon of Kerr black hole is significantly smaller than the event horizon of quantum corrected Kerr black hole. Moreover, the extremal quantum corrected Kerr black hole has spin ∼0.4952 which is marginally less than half of the extremal spin of Kerr black hole.

3 Unstable null orbits and black hole shadow

The photons emerging from a bright source may get trapped in unstable and stable circular null orbits in the vicinity of a black hole. Some of them in the unstable orbits fall into the event horizon, while the rest scatter away to the infinity. This is how the optical image of the black hole is formed, termed as shadow [93,94]. These orbits are characterized by an effective potential function. Therefore, we derive the null geodesic equations to study the effective potential and shadows of quantum corrected Kerr black hole in effective LQG, in order to understand the influence of LQG via Barbero–Immirzi parameter in terms of unstable orbits and optical images. For the quantum corrected Kerr black hole in effective LQG, the null geodesic equations can be obtained by employing the Hamilton–Jacobi formalism [95] which has been widely incorporated in the literature over the years. One can also begin with the Lagrangian or Hamiltonian methods, generating two constants of motion, the energy E and the angular momentum L along with mass of the particle under motion. The geodesic equations become completely integrable if we introduce a fourth constant of motion. The separation of variables arising in Hamilton–Jacobi formalism enables us to introduce a constant known as the Carter constant [95]. We consider the Hamilton–Jacobi equation

$$2\partial_\tau S = -g^{\mu\nu}\partial_{x^\mu} S \partial_{x^\nu} S \tag{11}$$

with the Jacobi action of the form

$$S = \frac{1}{2}m_{\text{p}}^2\tau - Et + L\phi + A_r(r) + A_\theta(\theta), \tag{12}$$

where, τ being the proper time is considered as an affine parameter and $m_{\text{p}} = 0$ is the photon mass. The functions $A_r(r)$ and $A_\theta(\theta)$ are arbitrary functions that can be determined easily (for complete derivation, see Ref. [95]). The constants $E = -p_t$ and $L = p_\phi$ can be obtained from the relation $p_\mu = g_{\mu\nu}\dot{x}^\nu$. Since, the three constants of motion, namely, mass of the particle, its energy and angular momentum can be derived from Lagrangian or Hamiltonian

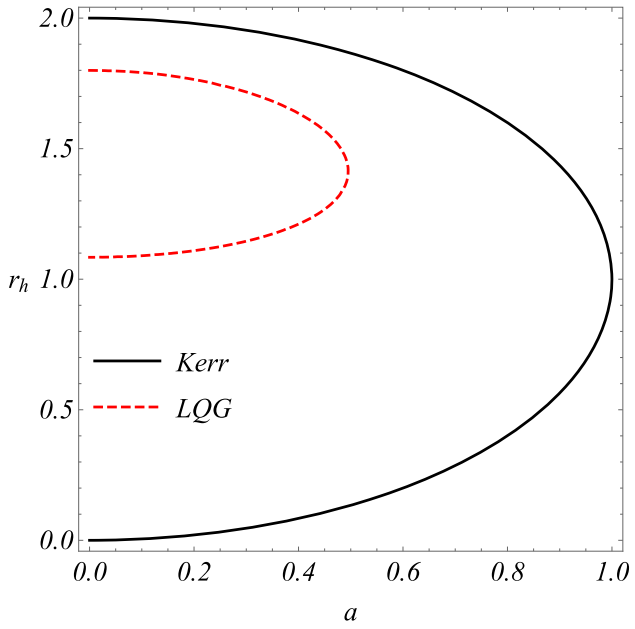

Fig. 1 Horizon structure of Kerr and quantum corrected Kerr black holes with respect to a for $M = 1$ and $\alpha \approx 1.1663$

methods. However, for the fourth constant, Hamilton–Jacobi method is introduced with Jacobi action assuming two arbitrary functions. These functions are considered dependent on r and θ because the associated fourth constant of motion must appear from the radial and θ-equations. Ultimately, the geodesic equations come out to be of the usual form as for the Kerr metric given as [94]

$$\rho^2 \dot{t} = \frac{r^2+a^2}{\Delta(r)}\left(E\left(r^2+a^2\right)-aL\right)+a\left(L-aE\sin^2\theta\right), \tag{13}$$

$$\rho^2 \dot{r} = \pm\sqrt{\mathcal{R}(r)}, \tag{14}$$

$$\rho^2 \dot{\theta} = \pm\sqrt{\Theta(\theta)}, \tag{15}$$

$$\rho^2 \dot{\phi} = \frac{a}{\Delta(r)}\left(E\left(r^2+a^2\right)-aL\right)+\left(L\csc^2\theta-aE\right), \tag{16}$$

where,

$$\mathcal{R}(r) = \left(\left(r^2+a^2\right)E-aL\right)^2-\Delta(r)\left(\mathcal{Z}+(L-aE)^2\right), \tag{17}$$

$$\Theta(\theta) = \mathcal{Z}+\cos^2\theta\left(a^2E^2-L^2\csc^2\theta\right), \tag{18}$$

where, $\mathcal{Z}$ denotes the Carter constant. The function $\mathcal{R}(r)$ is of prime importance in studying the effective potential and behavior of unstable orbits as it connects the radial geodesic equation with the effective potential, that is $\dot{r}^2 + 2V^{\text{eff}}(r) = 0$. In this case, for equatorial trajectories, it can also be expressed as

$$\begin{aligned}\mathcal{R}(r) &= -2r^4 V^{\text{eff}}(r)\\ &= \mathcal{R}_{\text{Kerr}}(r) - \frac{\alpha\left(\mathcal{Z}+(L-aE)^2\right)M^2}{r^2},\end{aligned} \tag{19}$$

where, the second term on right hand side of Eq. (19) is the deviation factor of $\mathcal{R}(r)$ from $\mathcal{R}_{\text{Kerr}}(r)$. The deviation in the metric function is fixed as it is independent of free parameters, however, the deviation in $\mathcal{R}(r)$ is dependent on a due to which it varies for each case of black hole spin. Note that the quantum correction does not affect the function $\Theta(\theta)$. The photon moving in a circular orbit is subjected to centripetal force to keep it in its orbit with an opposing force called the centrifugal force. The centrifugal force corresponds to a potential known as centrifugal potential that together with real potential makes up the effective potential. From the radial null geodesic equation, it can be written in terms of effective potential for Kerr black hole for equatorial trajectories as

$$V^{\text{eff}}(r) = V^{\text{eff}}_{\text{Kerr}}(r) + \frac{\alpha\left(\mathcal{Z}+(L-aE)^2\right)M^2}{2r^6}. \tag{20}$$

As in the case of $\mathcal{R}(r)$, the quantum correction term in the effective potential also depends on spin a that causes a variable deformation in the null orbits. This deviation is generally in terms of either shrinking or expansion of null orbits. However, depending on the type of spacetime metric, the shape of deformation term in metric function and effective potential functions, we can determine whether the null orbits shrink or expand. For a concrete and robust result under certain assumptions, we establish a theorem and present a simple proof to it as follows:

Theorem Suppose a Kerr-like metric described by $\Delta(r) = \Delta_{\text{Kerr}}(r) + b_1 r^p$ with $V^{\text{eff}}(r) = V^{\text{eff}}_{\text{Kerr}}(r) + b_2 r^q$ such that r^p and r^q be decreasing functions in an open interval $\mathcal{I} = (0, s) \subseteq \mathbb{R}^+$, and $b_1, b_2 \in \mathbb{R}^+$. If an unstable null orbit for Kerr black hole exists at a radial distance $r_k \in \mathcal{I}$, then the unstable null orbit corresponding to $\Delta(r)$ exists at some $r_0 \in \mathcal{I}$ such that $r_0 < r_k$.

Proof Given that $\Delta(r) = \Delta_{\text{Kerr}}(r) + b_1 r^p$ and $V^{\text{eff}}(r) = V^{\text{eff}}_{\text{Kerr}}(r) + b_2 r^q$ with decreasing functions r^p and r^q such that $p, q \in \mathbb{R}^-$, and $b_1, b_2 \in \mathbb{R}^+$ depend only on spin a. Now, if an unstable null orbit for Kerr black hole exists at some $r_k \in \mathcal{I}$, then the function $V^{\text{eff}}_{\text{Kerr}}(r)$ is concave at r_k that is $\partial_r^2 V^{\text{eff}}_{\text{Kerr}}(r_k) < 0$ and $\partial_r V^{\text{eff}}_{\text{Kerr}}(r_k) = 0$. Since, r^q is decreasing $\forall\ r \in \mathcal{I}$, therefore, $\partial_r V^{\text{eff}}(r_k) < 0$. From this, one of the following two possibilities holds:

(i) If $V^{\text{eff}}(r)$ is concave at r_0, then $\exists\, r_0 \in \mathcal{I}$ such that $r_0 < r_k$ and $\partial_r V^{\text{eff}}(r_0) = 0$.
(ii) If $V^{\text{eff}}(r)$ is convex at r_0, then $\exists\, r_0 \in \mathcal{I}$ such that $r_0 > r_k$ and $\partial_r V^{\text{eff}}(r_0) = 0$.

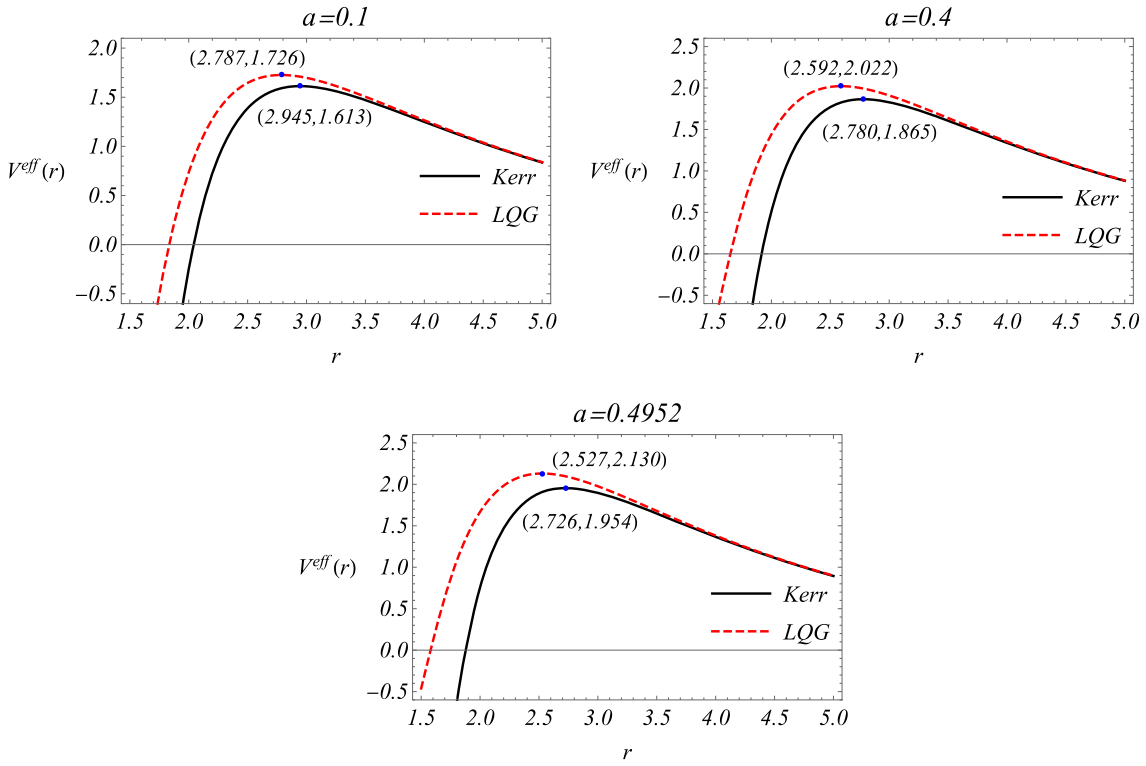

Fig. 2 Behavior of effective potential and unstable null orbits for Kerr and quantum corrected Kerr black holes for different values of a with $M = 1$ and $\alpha \approx 1.1663$

To prove the theorem, we either prove (i) holds or (ii) does not hold. Contrarily suppose that (ii) holds, then $\partial_r V^{\text{eff}}_{\text{Kerr}}(r_0) > 0$ but $V^{\text{eff}}_{\text{Kerr}}(r)$ must be decreasing at r_0 under the given statement. This gives a contradiction which implies that (ii) does not hold and thus (i) holds automatically. Therefore, it proves that the unstable null orbits shrink under the given assumptions. Note that we have not proved $r_0 \in \mathcal{I}$. Since, the lower bound of the interval $\mathcal{I}$ is 0 and $r_0 < r_k$, therefore, $r_0 \in \mathcal{I}$. We have also omitted the case when $r_0 = r_k$ because $b_1, b_2 \neq 0$. Moreover, the interval $\mathcal{I}$ is arbitrary and may have multiple extrema, however, the local maximum corresponding to the unstable orbit is unique.

The result proved in the above theorem can be viewed in Fig. 2 in terms of location of peaks of the curves. That is, the unstable null orbits for quantum corrected Kerr black hole are smaller than the unstable null orbits for Kerr black hole for all cases. Moreover, for each case of extremal spin of quantum corrected Kerr black hole, the difference between the sizes of unstable orbits for both black holes increases, which is specifically due to the presence of spin parameter in the deviation term in Eq. (20). Furthermore, with increase in spin, the unstable orbits of quantum corrected and Kerr black holes shrink.

The effective potential function governs the behavior of timelike and null orbits around a black hole. Whereas, the types of these orbits, whether stable or unstable, are determined mathematically by solving the equations $V^{\text{eff}}(r_{\text{p}}) = 0 = \partial_r V^{\text{eff}}(r_{\text{p}})$ and then identifying the concavity or convexity of the function as $\partial_r^2 V^{\text{eff}}(r_{\text{p}}) < 0$ for unstable orbits or $\partial_r^2 V^{\text{eff}}(r_{\text{p}}) > 0$ for stable orbits. Since, the photons are trapped in circular orbits and these orbits together in all orientations make up a sphere whose radius is denoted by r_{p}. On the surface of sphere, the radial component of these photons satisfies the equation $r = constant$. Therefore, we have $\dot{r} = 0 = \ddot{r}$ which is equivalent to $\mathcal{R}(r_{\text{p}}) = 0 = \partial_r \mathcal{R}(r_{\text{p}})$ by Eq. (14). Hence, solving the equations for critical orbits in terms of effective potential is equivalent to solving in terms of $\mathcal{R}(r)$. These equations give the values of impact parameters $\xi = L/E$ and $\eta = \mathcal{Z}/E^2$ as a function of arbitrary r_{p} given as

$$\xi(r_{\text{p}}) = \xi_{\text{Kerr}}(r_{\text{p}}) + \frac{2\alpha M^2 r_{\text{p}} \left(\Delta_{\text{Kerr}}(r_{\text{p}}) + r_{\text{p}}\Gamma\right)}{a\Gamma\left(\alpha M^2 - r_{\text{p}}^3\Gamma\right)}, \tag{21}$$

$$\eta(r_{\text{p}}) = \eta_{\text{Kerr}}(r_{\text{p}}) + \frac{4\alpha M^2 r_{\text{p}}^3}{\Gamma^2\left(\alpha M^2 - \Gamma r_{\text{p}}^3\right)^2}\Bigg[2\Gamma r_{\text{p}}^3(M-\Gamma) - \alpha M^3 + \frac{r_{\text{p}}^2(M-2\Gamma)\left[M\left(\alpha M - 3r_{\text{p}}^2\Gamma\right) + \Gamma r_{\text{p}}^3\right]}{a^2}\Bigg], \tag{22}$$

where, $\Gamma = r_{\rm p} - M$. For $\alpha = 0$, the quantum correction terms in Eqs. (21) and (22) vanish, and the impact parameters for Kerr black hole are recovered. These impact parameters then determine the celestial coordinates [96]

$$X(r_{\rm p}) = -\lim_{\substack{r\to\infty\\ \theta\to\theta_0}} r^2 \sin\theta \frac{d\phi}{dr}, \quad Y(r_{\rm p}) = \lim_{\substack{r\to\infty\\ \theta\to\theta_0}} r^2 \frac{d\theta}{dr} \tag{23}$$

to sketch a projective 2D image of the black hole shadow, given in the form

$$X(r_{\rm p}) = -\xi(r_{\rm p}) \csc\theta_0, \tag{24}$$

$$Y(r_{\rm p}) = \pm\sqrt{\eta(r_{\rm p}) + a^2\cos^2\theta_0 - \xi^2(r_{\rm p})\cot^2\theta_0}. \tag{25}$$

The limits in Eq. (23) correspond to the radial and angular components of observer's location. For an equatorial observer, the celestial coordinates reduce to

$$X(r_{\rm p}) = -\xi(r_{\rm p}), \quad Y(r_{\rm p}) = \pm\sqrt{\eta(r_{\rm p})}. \tag{26}$$

Since, the shadows are formed as circular contours and often deformed for the rotating black hole cases. Therefore, one can assume the condition $Y(r_{\rm p}) = 0$ corresponding to the extreme points on the shadow contour on the X-axis of the celestial plane which ultimately correspond to the extreme values of the interval $[r_{\rm p}^{\rm min}, r_{\rm p}^{\rm max}]$ for the photon sphere. However, the photon sphere around a static black hole has a unique width which cannot be considered as a parameter. To deal with this, one can modify the impact parameter η in the form $\eta_{\rm m} = \left(\mathcal{Z} + (L - aE)^2\right)/E^2$ and consider ξ as the parameter. The extreme values of the interval containing ξ are determined by solving the equation $\Theta(\theta_0) = 0$. The celestial coordinates in Eq. (26) can also be expressed as □

$$X(r_{\rm p}) = X_{\rm Kerr}(r_{\rm p}) - \frac{2\alpha M^2 r_{\rm p}\left(\Delta_{\rm Kerr}(r_{\rm p}) + r_{\rm p}\Gamma\right)}{a\Gamma\left(\alpha M^2 - r_{\rm p}^3\Gamma\right)}, \tag{27}$$

$$\begin{aligned} Y(r_{\rm p}) = Y_{\rm Kerr}(r_{\rm p}) &\pm \frac{2\alpha M^2 r_{\rm p}^3}{\Gamma^2\sqrt{\eta_{\rm Kerr}(r_{\rm p})}\left(\alpha M^2 - \Gamma r_{\rm p}^3\right)^2} \\ &\times\left[\frac{r_{\rm p}^2(M-2\Gamma)\left[M\left(\alpha M - 3r_{\rm p}^2\Gamma\right) + \Gamma r_{\rm p}^3\right]}{a^2}\right. \\ &\left. + 2\Gamma r_{\rm p}^3(M-\Gamma) - \alpha M^3\right] \mp \text{higher order terms}, \end{aligned} \tag{28}$$

which further reduce to the celestial coordinates for Kerr black hole under the limit $\alpha = 0$. The extra terms on the right hand side of Eqs. (27) and (28) describe the deviation of shadow due to LQG effects from the shadow of Kerr black hole. The Y-coordinate in Eq. (28) is expressed in terms of an alternating infinite series contributing to the deviation of the shadow from the shadow of Kerr black hole. To quantify this deviation in the shadow, we plot some shadow contours for a few cases of spin parameter values as given in Fig. 3. From the difference of sizes of the Kerr and quantum corrected Kerr black holes for all cases, one can deduce that the quantum corrected Kerr black hole will appear smaller to a visualizing observer at infinity as compared to the Kerr black hole. As the value of spin parameter increases, the distortion starts appearing in the shadows of quantum corrected Kerr black hole. That is, the difference between the shadow contours on the left side increases with increase in spin. It suggests that the spin parameter influences the elongation of shadows for quantum corrected Kerr black hole more than the Kerr black hole up to $a = 0.4952$. The third plot with three contours show a huge difference between the shadows of quantum corrected and Kerr black holes for their respective extreme spin values. Therefore, one may not expect to visualize a perfectly flattened shadow for extreme quantum corrected Kerr black hole. Moreover, the deviation in shadow contours for $a = 0.4952$ for both black holes can also be measured. For smaller values of spin, both black holes are centered closer to the origin and will certainly be centered at origin for $a = 0$.

4 Constraints on spin parameter

In this section, we will explore the constraints on the spin parameter a for both Kerr and quantum corrected Kerr black holes, using observational data from the EHT collaborations. These observations, focusing on M87* and Sgr A*, will allow us to determine the limits on the spin values of these black holes. We will compare the constraints obtained for both black holes to gain insights into how LQG might influence the characteristics of the rotating black hole, providing a deeper understanding of the potential effects of quantum gravity on black holes. To do this, we calculate the angular radii of the shadows of both black holes to establish a comparative analysis with the angular radii of M87* and Sgr A*. Corresponding to such a bound on the spin parameter, the black hole is considered to mimic either M87* or Sgr A* if the angular diameter of black hole shadow falls within 1-σ interval. This study specifically examines rotating black holes, as supermassive black holes are naturally expected to exhibit significant rotational features due to their formation and evolution processes. A coordinate-independent formalism, commonly referred to as the Kumar–Ghosh method [97,98], is employed, where the shadow area is utilized which is defined as

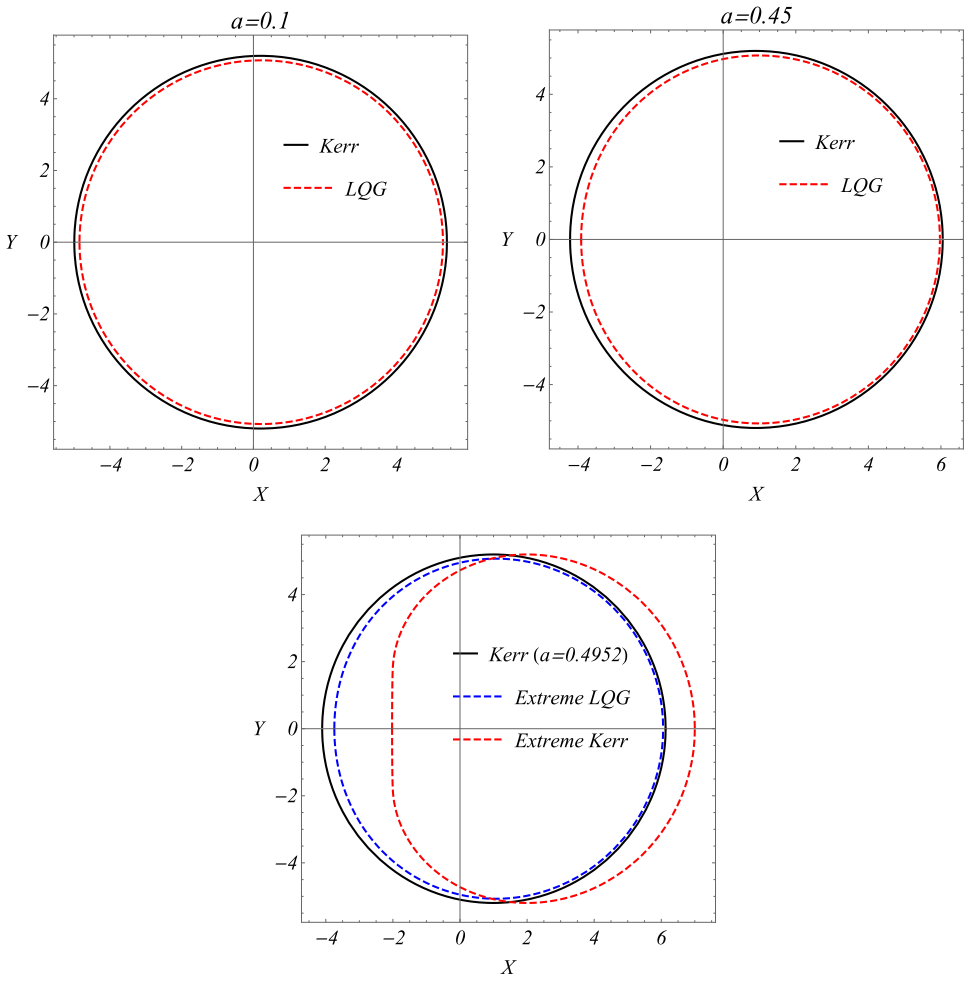

Fig. 3 Behavior of shadows for Kerr and quantum corrected Kerr black holes for different values of a with $M = 1$ and $\alpha \approx 1.1663$, visualized by an equatorial observer at radial infinity

$$A_{\rm sh} = 2\int_{r_-}^{r_+} dx^r\, Y(r)\partial_r X(r). \tag{29}$$

The values r_+ and r_- represent the size of the retrograde and prograde stable circular orbits as measured from the origin, respectively. Suppose that the separation between the black hole and observer is described by the linear distance d, then the diameter of the black hole shadow is measured as [54,99]

$$\theta_{\rm d} = \frac{2}{d}\sqrt{\frac{A_{\rm sh}}{\pi}}. \tag{30}$$

By utilizing the relations (29) and (30), the angular diameter of the black hole shadow can be written in terms of spin a, $r_{\rm p}$ and θ_0. For the comparison of the shadows, the EHT data determines the distance d of Earth from M87* and Sgr A*, the mass M and the shadow size $\theta_{\rm d}$ of M87* and Sgr A*. For M87*, we get $d = 16.8$Mpc, $M = 6.5 \times 10^9 {\rm M}_\odot$ and $\theta_{\rm d} = 42 \pm 3\,\mu$as [31,100,101]. Whereas, for Sgr A*, we get $d = 8$kpc, $M = 4 \times 10^6 {\rm M}_\odot$ and $\theta_{\rm d} = 48.7 \pm 7\,\mu$as [102,103]. Here, ${\rm M}_\odot$ denotes the solar mass, kpc and Mpc stand for kilo and mega parsec, and μas stands for micro arcsec. For simplicity, we have not considered uncertainties in the measurements of mass and distance. The EHT conducted the observations at the inclination angles of 17° for M87* and $< 50°$ for Sgr A*. Therefore, we will also consider the angles of 17° for M87* and 45° for Sgr A* for the calculations of shadows.

The impact of LQG that deviates the quantum corrected Kerr black hole from Kerr black hole is obvious in Fig. 4. We have plotted the shadow angular diameters of the Kerr and quantum corrected Kerr black holes with respect to spin a and compared it with M87* and Sgr A*. The 1-σ uncertainty levels are indicated by dark gray regions. For the comparison with M87*, we found that the shadow diameter of Kerr black hole lies within 1-σ uncertainty level for $0 \leq a \lesssim 0.586$, while, for other values of a, the shadow diameter of Kerr black hole lies within 2-σ uncertainty level. The upper bound of spin is denoted by $a_{\rm max} \approx 0.586$ at which the transition of shadow diameter is observed from 1-σ level to 2-σ. Therefore, the Kerr black hole can be regarded identical with M87* for $0 \leq a \lesssim 0.586$. However, the quantum corrected Kerr black hole does not mimic M87* as its shadow diameter lies within 2-σ uncertainty level for all values of spin which is a tremendous impact of LQG on quantum corrected Kerr

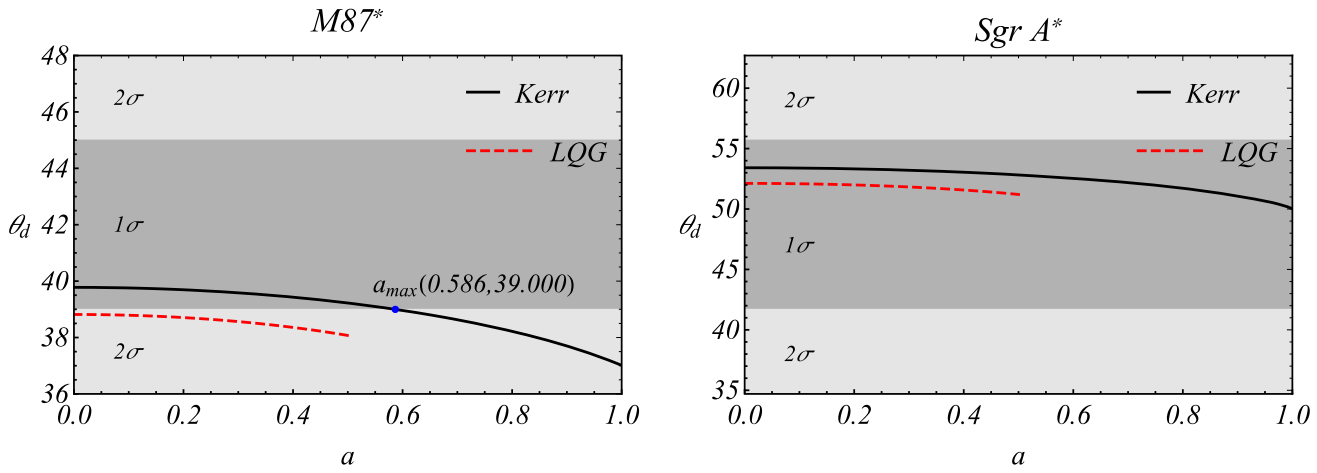

Fig. 4 Comparison of shadow angular diameter $\theta_{\rm d}$ for quantum corrected Kerr black hole (dashed red curve) and Kerr black hole (solid black curves) with the EHT data for M87* (at inclination angle of 17°) and Sgr A* (at inclination angle of 45°) for the bounds on spin a within 1-σ intervals

black hole. Generally, the 2-σ uncertainty level is also considered for the comparison, however, we ignore this region in order to reduce the possibility of uncertainty. This essentially eliminates the possibility for the quantum corrected Kerr black hole to behave like M87*. However, an entirely opposite impact of LQG is visualized for the case of Sgr A*. The Kerr black hole behaves identical with Sgr A* for all values of spin as its shadow diameter lies within 1-σ uncertainty level and $\theta_{\rm d}$ approaches the median value 48.7 μas as a approaches its maximal value. For the quantum corrected Kerr black hole, the shadow diameter also lies within 1-σ uncertainty level. However, under the influence of LQG, the shadow diameter for quantum corrected Kerr black hole is closer to the median value 48.7 μas for each value of spin. Therefore, one may regard the quantum corrected Kerr black hole to mimic Sgr A* for all values of spin which is more likely than the Kerr black hole within its interval of spin.

5 Effect of plasma on shadow

We know that astrophysical black holes are generally surrounded by plasma. Moreover, excited states of matter at high temperatures with their constituent particles (positive and negative charges) may have significant impact on the quantum corrected Kerr black hole at Planck scales. This being an important aspect in theoretical physics, we investigate the influence of plasma on the appearance of quantum corrected Kerr black hole. We consider pressureless and non-magnetized plasma with distribution functions dependent on r and θ. We begin by considering the plasma electron frequency defined as

$$\omega_{\rm p}(r,\theta) = \frac{4\pi e^2}{m_{\rm e}} N_{\rm e}(r,\theta) \tag{31}$$

that modifies the Hamiltonian describing the photon motion in a plasma medium given as [70]

$$\mathcal{H} = \frac{1}{2}\left[g^{\mu\nu}p_\mu p_\nu + \omega_{\rm p}^2(r,\theta)\right], \tag{32}$$

where $e, m_{\rm e}$ and $N_{\rm e}$ are the charge, mass and number density of the electron, respectively. The plasma electron frequency is related to the refractive index $n(r,\theta)$ as

$$n(r,\theta) = \sqrt{1 - \frac{\omega_{\rm p}^2(r,\theta)}{\omega^2(r,\theta)}}, \tag{33}$$

where $\omega(r,\theta)$ is the frequency of photon measured by a static observer outside the event horizon. The Hamilton's equations are defined as

$$\dot{x}^\mu = \partial_\tau x^\mu = \partial_{p_\mu}\mathcal{H}, \qquad \dot{p}_\mu = \partial_\tau p_\mu = -\partial_{x^\mu}\mathcal{H} \tag{34}$$

with τ being an affine parameter. Since, a plasma medium is dense and dispersive, therefore, the motion of photons is affected by the frequencies of electrons in the plasma. Therefore, the frequency of the propagating photon must be greater than the frequency of the electrons in plasma, that is, $\omega^2(r,\theta) \geq \omega_{\rm p}^2(r,\theta)$. The observer is assumed static with the four-velocity in comoving coordinates given as $U^\mu(r,\theta) = (-g_{tt}(r,\theta))^{-1/2}$ and the photon frequency is $\omega(r,\theta) = -p_\mu U^\mu(r,\theta) = -p_t U^t(r,\theta)$. The Planck's relation connects the energy and the angular frequency as $E = \hbar\omega_0$ which gives $p_t = -\omega_0$ by setting the units for $\hbar = 1$. Therefore, one obtains

$$\omega(r,\theta) = \omega_0\left(-g_{tt}(r,\theta)\right)^{-\frac{1}{2}}. \tag{35}$$

We obtain t and ϕ components of geodesic equations corresponding to two constants of motion, energy E and angular momentum L. For other two equations, we consider

Hamilton–Jacobi equation in the form

$$g^{\mu\nu}\partial_{x^\mu}\mathcal{S}\partial_{x^\nu}\mathcal{S}+\omega_{\rm p}^2(r,\theta)=0 \tag{36}$$

with Jacobi action given by Eq. (12) with $m_{\rm p}=0$ as the third constant of motion. For the given metric, the Hamilton–Jacobi equation

$$\begin{aligned}&\Delta(r)\left(\partial_r\mathcal{A}_r(r)\right)^2+\left(L^2\csc^2\theta-a^2E^2\right)\cos^2\theta\\&+(L-aE)^2+\left(\partial_\theta\mathcal{A}_\theta(\theta)\right)^2-\frac{\left(\left(r^2+a^2\right)E-aL\right)^2}{\Delta(r)}\\&+\rho^2\omega_{\rm p}^2(r,\theta)=0\end{aligned} \tag{37}$$

cannot be separated until we assume [70]

$$\omega_{\rm p}(r,\theta)=\frac{\sqrt{f_r(r)+f_\theta(\theta)}}{\rho}, \tag{38}$$

where, $f_r(r)$ and $f_\theta(\theta)$ are arbitrary functions that ensures the separability of the Eq. (37). Therefore, generating the Carter constant $\mathcal{Z}$ as fourth constant of motion, the null geodesic equations are of same form as Eqs. (13)-(16) but with the functions

$$\begin{aligned}\mathcal{R}(r)=&\left(aL-\left(r^2+a^2\right)E\right)^2\\&-\Delta(r)\left(f_r(r)+\mathcal{Z}+(aE-L)^2\right),\end{aligned} \tag{39}$$

$$\Theta(\theta)=\mathcal{Z}+a^2E^2\cos^2\theta-L^2\cot^2\theta-f_\theta(\theta). \tag{40}$$

The impact parameters ξ and η in presence of plasma become

$$\begin{aligned}\xi(r_{\rm p})=&\frac{1}{a\Delta'(r_{\rm p})}\Big[\left(r_{\rm p}^2+a^2\right)\Delta'(r_{\rm p})-\Delta(r_{\rm p})\Big(2r_{\rm p}\\&+\sqrt{4r_{\rm p}^2-f_r'(r_{\rm p})\Delta'(r_{\rm p})}\Big)\Big],\end{aligned} \tag{41}$$

$$\begin{aligned}\eta(r_{\rm p})=&\frac{1}{a^2\Delta'^2(r_{\rm p})}\Big[8r_{\rm p}^2\Delta(r_{\rm p})\left[a^2-\Delta(r_{\rm p})\right]-\left[r_{\rm p}^4\right.\\&\left.+a^2f_r(r_{\rm p})\right]\Delta'^2(r_{\rm p})+\left[4r_{\rm p}^3-\left(a^2\right.\right.\\&\left.\left.-\Delta(r_{\rm p})\right)f_r'(r_{\rm p})\right]\Delta(r_{\rm p})\Delta'(r_{\rm p})+2r_{\rm p}\Delta(r_{\rm p})\Big[2\Big(a^2\\&-\Delta(r_{\rm p})\Big)+r_{\rm p}\Delta'(r_{\rm p})\Big]\sqrt{4r_{\rm p}^2-f_r'(r_{\rm p})\Delta'(r_{\rm p})}\Big].\end{aligned} \tag{42}$$

Now considering two cases for the functions $f_r(r)$ and $f_\theta(\theta)$, we will construct celestial coordinates to investigate shadows. The case I corresponds to the assumption $f_r(r)=\omega_{\rm c}^2\sqrt{M^3r}$ and $f_\theta(\theta)=0$, where, ω_c has the dimensions of frequency. The celestial coordinates for this case are of the same form as in Eqs. (24) and (25) with their respective impact parameters given in Eqs. (41) and (42). For the equatorial observer, the celestial coordinates reduce to the same form as in Eq. (26). The **case II** corresponds to the assumption $f_r(r)=0$ and $f_\theta(\theta)=\omega_{\rm c}^2M^2\left(1+2\sin^2\theta\right)$ with the same parameter ω_c. The horizontal component of the celestial coordinates for this case is of the same form as in Eq. (24), however, the vertical component is modified. For an observer at (∞,θ_0), it becomes

$$\begin{aligned}Y(r_{\rm p})=\pm\Big[&\eta(r_{\rm p})+a^2\cos^2\theta_0-\xi^2(r_{\rm p})\cot^2\theta_0\\&-\omega_{\rm c}^2M^2\left(1+2\sin^2\theta_0\right)\Big]^{\frac{1}{2}}\end{aligned} \tag{43}$$

and for the equatorial observer, it reduces to

$$Y(r_{\rm p})=\pm\sqrt{\eta(r_{\rm p})-3\omega_{\rm c}^2M^2}. \tag{44}$$

For both of above mentioned cases, we have plotted the shadows in Fig. 5 for a few values of plasma parameter $\omega_{\rm c}$ and keeping a fixed spin of the quantum corrected Kerr black hole. The spin deviates the shadow from a pure circular loop causing a distortion. While, the plasma parameter $\omega_{\rm c}$ reduces the size of the shadow. It can also be seen that $\omega_{\rm c}$ in case II is more significant and has higher sensitivity as compared to the case I. The variation in the shadow size for case II is greater than the variation observed in case I.

6 Discussion

By a smooth matching of APS and qOS spacetimes by identifying a set of suitable coordinate transformation, a quantum corrected Schwarzschild black hole in LQG is obtained with a relatively weak extra term of order r^{-4} depending on Barbero–Immirzi parameter γ [28]. During the collapse of the dust ball, corresponding to a lower bound of the radial coordinate, a lower bound on the mass of this black hole is obtained, below which, there exists no horizon, whereas, a two horizon system is obtained for all mass values above the minimum mass limit. Ye et al. [29] studied the shadows of this black hole to determine the effect of LQG on the black hole. They considered the fixed value of the Barbero–Immirzi parameter and hence the parameter α. They presented their findings in comparison with the results of Schwarzschild black hole. Motivated by this, we considered the rotating counterpart of the quantum corrected Schwarzschild black hole, in effective LQG and accomplished our analysis in comparison with the results for Kerr black hole.

The rotating black hole metric (7) being an effective metric still encompasses various features of Kerr-like black hole, especially the existence of time translation and rotational invariance isometries. Additionally, on removing the spin, its exact static counterpart is recovered, and on removing the quantum effects, the rotating metric reduces to Kerr metric and the static metric reduces to Schwarzschild metric. The parameter α though appears as the LQG parameter in the black hole metric, however, it does not behave as a free parameter and has a fixed value that cannot be varied. The metric function of the quantum corrected Kerr black hole is

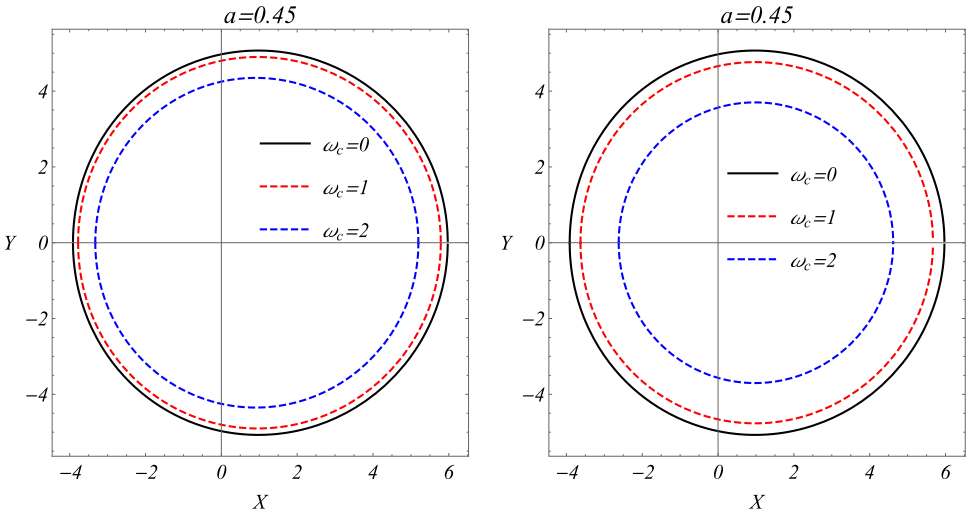

Fig. 5 Influence of ω_c in case I (left panel) and case II (right panel) on shadows of quantum corrected Kerr black hole for a fixed value of a

expressed in terms of the metric function of Kerr black hole for which the effect of LQG can be observed in the Eq. (10) and from the Fig. 1. The quantum corrected Kerr black hole in effective LQG also exhibits two horizons, though the event horizon being small as compared to the event horizon of Kerr black hole, reduces the size of black hole due to LQG effects. Its extreme spin value is also reduced to the half of extreme spin of Kerr black hole.

The function $\mathcal{R}(r)$ plays a vital role in particle orbits and shadow analysis. Like the metric function, it is also expressed in terms of the function corresponding to the Kerr black hole which generates an identical form of effective potential as well. This form enables us to generalize the location of unstable null orbits for such kind of metrics. We proved a theorem based on convexity and the familiar results of effective potential of Kerr black hole, which ensures that the unstable orbits for such a quantum corrected Kerr black hole will be smaller than the unstable orbits for Kerr black hole. This result holds true only if the extra term in effective potential function is decreasing function of r. The result in this theorem is then verified numerically in the Fig. 2. The impact parameters and celestial coordinates for quantum corrected Kerr black hole are also expressed in terms of the impact parameters and celestial coordinates for Kerr black hole. The deviation terms in the celestial coordinates determine the deviation of shadow of quantum corrected Kerr black hole from the shadow of Kerr black hole. The LQG effects influences both the size of the shadow and the distortion in it. Since, the extreme spin for quantum corrected Kerr black hole is $\sim$0.4952, so the ergosphere does not get enough strength to create a flat shadow like the shadow of Kerr black hole.

The astrophysical impact of LQG on quantum corrected Kerr black hole is investigated through the comparison of the shadow size for Kerr and quantum corrected Kerr black holes with the size of M87* and Sgr A*. Along with the images, the data from EHT results enabled us to draw an analysis to determine the constraints on the black hole spin parameters and the influence of LQG on it. The Kerr black hole is defined for $0 \leq a \leq 1$, however, it becomes identical with M87* for $0 \leq a \leq 0.586$. Whereas, the effect of LQG on quantum corrected Kerr black hole inhibits it to behave like M87* for all spin values. On the other hand, both Kerr and quantum corrected Kerr black holes mimic Sgr A* for all spin values, however, due to LQG effects, the quantum corrected Kerr black hole is more likely to mimic Sgr A* than Kerr black hole.

The plasma surrounding the quantum corrected Kerr black hole in effective LQG has a great impact on the light propagation. The shadow size is reduced by increasing the value of ω_c in both cases. However, the quantity of variation in shadow size reveals that ω_c in case II is more sensitive and has greater impact than that in case I.

This study can be further extended to understand the influence of plasma and LQG on each other in the vicinity of M87* and Sgr A*. As a future project, one may also investigate the effect of LQG on the deflection of light in strong and weak regimes of quantum corrected Kerr black hole. The study of black hole evaporation rate, Hawking radiation via tunneling process and Unruh effect would also be an intriguing analysis. Moreover, it will be interesting to study the effect of LQG on the quantum corrected Kerr black hole behaving as a particle accelerator.

Acknowledgements This paper is dedicated to the memory of Prof. Jerzy Lewandowski, who derived the static quantum corrected black hole metric in LQG which is considered in this paper. He is no more with us but his work will continue to inspire us, leaving a lasting legacy in theoretical physics. We are thankful to Francesco Fazzini for discussions and useful suggestions for improvements in the paper.

Data Availability Statement This manuscript has no associated data. [Author's comment: Data sharing not applicable to this article as no datasets were generated or analyzed during the current study.]

Code Availability Statement This manuscript has no associated code/software. [Author's comment: Code/Software sharing not appli-

cable to this article as no code/software were generated or analyzed during the current study.]

Funded by SCOAP[3].

References

1. K. Schwarzschild, Sitzungsberichte der Koeniglich-Preussischen Akademie der Wissenschaften, 189 (1916)
2. P.S. Joshi, Pramana **55**, 529 (2000). https://doi.org/10.1007/s12043-000-0164-4. arXiv:gr-qc/0006101 [gr-qc]
3. R. Penrose, Phys. Rev. Lett. **14**, 57 (1965). https://doi.org/10.1103/PhysRevLett.14.57
4. S.W. Hawking, R. Penrose, Proc. R. Soc. Lond. Ser. A **314**, 529 (1970). https://doi.org/10.1098/rspa.1970.0021
5. C. Rovelli, *Quantum Gravity*, Cambridge Monographs on Mathematical Physics (Cambridge University Press, Cambridge, 2004)
6. T. Thiemann, *Modern Canonical Quantum General Relativity*, Cambridge Monographs on Mathematical Physics (Cambridge University Press, Cambridge, 2007)
7. A. Ashtekar, J. Lewandowski, Class. Quantum Gravity **21**, R53 (2004). https://doi.org/10.1088/0264-9381/21/15/R01. arXiv:gr-qc/0404018 [gr-qc]
8. M. Han, Y. Ma, W. Huang, Int. J. Mod. Phys. D **16**, 1397 (2007). https://doi.org/10.1142/S0218271807010894. arXiv:gr-qc/0509064 [gr-qc]
9. A. Perez, Living Rev. Relativ. **16**, 3 (2013). https://doi.org/10.12942/lrr-2013-3. arXiv:1205.2019 [gr-qc]
10. M. Bojowald, Phys. Rev. Lett. **86**, 5227 (2001). https://doi.org/10.1103/PhysRevLett.86.5227
11. A. Ashtekar, M. Bojowald, J. Lewandowski (2003). https://doi.org/10.48550/arXiv.gr-qc/0304074. arXiv:gr-qc/0304074 [gr-qc]
12. A. Ashtekar, T. Pawlowski, P. Singh, Phys. Rev. Lett. **96**, 141301 (2006). https://doi.org/10.1103/PhysRevLett.96.141301
13. A. Ashtekar, T. Pawlowski, P. Singh, Phys. Rev. D **73**, 124038 (2006). https://doi.org/10.1103/PhysRevD.73.124038
14. A. Ashtekar, T. Pawlowski, P. Singh, Phys. Rev. D **74**, 084003 (2006). https://doi.org/10.1103/PhysRevD.74.084003
15. A. Ashtekar, M. Bojowald, Class. Quantum Gravity **23**, 391 (2006). https://doi.org/10.1088/0264-9381/23/2/008. arXiv:gr-qc/0509075 [gr-qc]
16. C.G. Böhmer, K. Vandersloot, Phys. Rev. D **76**, 104030 (2007). https://doi.org/10.1103/PhysRevD.76.104030
17. L. Modesto, Int. J. Theor. Phys. **49**, 1649 (2010). https://doi.org/10.1007/s10773-010-0346-x. arXiv:0811.2196 [gr-qc]
18. A. Corichi, P. Singh, Class. Quantum Gravity **33**, 055006 (2016). https://doi.org/10.1088/0264-9381/33/5/055006. arXiv:1506.08015 [gr-qc]
19. A. Ashtekar, J. Olmedo, P. Singh, Phys. Rev. Lett. **121**, 241301 (2018). https://doi.org/10.1103/PhysRevLett.121.241301
20. A. Ashtekar, J. Olmedo, P. Singh, Phys. Rev. D **98**, 126003 (2018). https://doi.org/10.1103/PhysRevD.98.126003
21. C. Zhang, Y. Ma, S. Song, X. Zhang, Phys. Rev. D **102**, 041502 (2020). https://doi.org/10.1103/PhysRevD.102.041502
22. C. Zhang, Y. Ma, S. Song, X. Zhang, Phys. Rev. D **105**, 024069 (2022). https://doi.org/10.1103/PhysRevD.105.024069
23. M. Bojowald, R. Goswami, R. Maartens, P. Singh, Phys. Rev. Lett. **95**, 091302 (2005). https://doi.org/10.1103/PhysRevLett.95.091302
24. M. Bojowald, J.D. Reyes, R. Tibrewala, Phys. Rev. D **80**, 084002 (2009). https://doi.org/10.1103/PhysRevD.80.084002
25. J. Münch, Phys. Rev. D **104**, 046019 (2021). https://doi.org/10.1103/PhysRevD.104.046019
26. V. Husain, J.G. Kelly, R. Santacruz, E. Wilson-Ewing, Phys. Rev. Lett. **128**, 121301 (2022). https://doi.org/10.1103/PhysRevLett.128.121301
27. K. Giesel, B.-F. Li, P. Singh, Phys. Rev. D **104**, 106017 (2021). https://doi.org/10.1103/PhysRevD.104.106017
28. J. Lewandowski, Y. Ma, J. Yang, C. Zhang, Phys. Rev. Lett. **130**, 101501 (2023). https://doi.org/10.1103/PhysRevLett.130.101501
29. J.-P. Ye, Z.-Q. He, A.-X. Zhou, Z.-Y. Huang, J.-H. Huang, Phys. Lett. B **851**, 138566 (2024). https://doi.org/10.1016/j.physletb.2024.138566
30. H. Falcke, F. Melia, E. Agol, Astrophys. J. **528**, L13 (2000). https://doi.org/10.1086/312423. arXiv:astro-ph/9912263 [astro-ph]
31. E.H.T. Collaboration, Astrophys. J. Lett. **875**, L1 (2019). https://doi.org/10.3847/2041-8213/ab0ec7
32. E.H.T. Collaboration, Astrophys. J. Lett. **875**, L4 (2019). https://doi.org/10.3847/2041-8213/ab0ec8
33. E.H.T. Collaboration, Astrophys. J. Lett. **930**, L12 (2022). https://doi.org/10.3847/2041-8213/ac6674
34. E.H.T. Collaboration, Astrophys. J. Lett. **930**, L14 (2022). https://doi.org/10.3847/2041-8213/ac6686
35. L. Amarilla, E.F. Eiroa, Phys. Rev. D **85**, 064019 (2012). https://doi.org/10.1103/PhysRevD.85.064019
36. L. Amarilla, E.F. Eiroa, Phys. Rev. D **87**, 044057 (2013). https://doi.org/10.1103/PhysRevD.87.044057
37. F. Atamurotov, A. Abdujabbarov, B. Ahmedov, Phys. Rev. D **88**, 064004 (2013). https://doi.org/10.1103/PhysRevD.88.064004
38. A. Grenzebach, V. Perlick, C. Lämmerzahl, Phys. Rev. D **89**, 124004 (2014). https://doi.org/10.1103/PhysRevD.89.124004
39. U. Papnoi, F. Atamurotov, S.G. Ghosh, B. Ahmedov, Phys. Rev. D **90**, 024073 (2014). https://doi.org/10.1103/PhysRevD.90.024073
40. F. Atamurotov, S.G. Ghosh, B. Ahmedov, Eur. Phys. J. C **76**, 273 (2016). https://doi.org/10.1140/epjc/s10052-016-4122-9. arXiv:1506.03690 [gr-qc]
41. O.Y. Tsupko, Phys. Rev. D **95**, 104058 (2017). https://doi.org/10.1103/PhysRevD.95.104058
42. P.V.P. Cunha, C.A.R. Herdeiro, Gen. Relativ. Gravit. **50**, 42 (2018). https://doi.org/10.1007/s10714-018-2361-9. arXiv:1801.00860 [gr-qc]
43. Y. Mizuno, Z. Younsi, C.M. Fromm, O. Porth, M. De Laurentis, H. Olivares, H. Falcke, M. Kramer, L. Rezzolla, Nat. Astron. **2**, 585 (2018). https://doi.org/10.1038/s41550-018-0449-5. arXiv:1804.05812 [astro-ph.GA]
44. U. Papnoi, F. Atamurotov, Phys. Dark Universe **35**, 100916 (2022). https://doi.org/10.1016/j.dark.2021.100916
45. F. Atamurotov, U. Papnoi, K. Jusufi, Class. Quantum Gravity **39**, 025014 (2021). https://doi.org/10.1088/1361-6382/ac3e76
46. F. Sarikulov, F. Atamurotov, A. Abdujabbarov, B. Ahmedov, Eur. Phys. J. C **82**, 771 (2022). https://doi.org/10.1140/epjc/s10052-022-10711-4
47. F. Atamurotov, I. Hussain, G. Mustafa, K. Jusufi, Eur. Phys. J. C **82**, 831 (2022). https://doi.org/10.1140/epjc/s10052-022-10782-3. arXiv:2209.01652 [gr-qc]

48. B. Rahmatov, M. Zahid, S.U. Khan, J. Rayimbaev, I. Ibragimov, Z. Yuldoshev, A. Dauletov, S. Muminov, Chin. Phys. C **49**, 075105 (2025). https://doi.org/10.1088/1674-1137/adc188
49. M. Afrin, S.G. Ghosh, Astrophys. J. **932**, 51 (2022). https://doi.org/10.3847/1538-4357/ac6dda
50. K. Jusufi, S. Capozziello, S. Bahamonde, M. Jamil, Eur. Phys. J. C **82**, 1018 (2022). https://doi.org/10.1140/epjc/s10052-022-10971-0. arXiv:2205.07629 [gr-qc]
51. R.C. Pantig, A. Övgün, Ann. Phys. **448**, 169197 (2023). https://doi.org/10.1016/j.aop.2022.169197
52. S. Hendi, K. Jafarzade, B.E. Panah, J. Cosmol. Astropart. Phys. **022**, 02 (2023). https://doi.org/10.1088/1475-7516/2023/02/022
53. S.U. Islam, J. Kumar, R.K. Walia, S.G. Ghosh, Astrophys. J. **943**, 22 (2023). https://doi.org/10.3847/1538-4357/aca411
54. M. Afrin, S. Vagnozzi, S.G. Ghosh, Astrophys. J. **944**, 149 (2023). https://doi.org/10.3847/1538-4357/acb334
55. R.C. Pantig, A. Övgün, D. Demir, Eur. Phys. J. C **83**, 250 (2023). https://doi.org/10.1140/epjc/s10052-023-11400-6. arXiv:2208.02969 [gr-qc]
56. A. Uniyal, R.C. Pantig, A. Övgün, Phys. Dark Univ. **40**, 101178 (2023). https://doi.org/10.1016/j.dark.2023.101178
57. K. Nozari, S. Saghafi, Eur. Phys. J. C **83**, 588 (2023). https://doi.org/10.1140/epjc/s10052-023-11755-w. arXiv:2305.17237 [gr-qc]
58. A. Davlataliev, B. Narzilloev, I. Hussain, A. Abdujabbarov, B. Ahmedov, Phys. Dark Univ. **42**, 101340 (2023). https://doi.org/10.1016/j.dark.2023.101340
59. K. Jafarzade, S.H. Hendi, M. Jamil, S. Bahamonde, Phys. Dark Univ. **45**, 101497 (2024). https://doi.org/10.1016/j.dark.2024.101497
60. C. Bambi, K. Freese, S. Vagnozzi, L. Visinelli, Phys. Rev. D **100**, 044057 (2019). https://doi.org/10.1103/PhysRevD.100.044057
61. Y. Hou, M. Guo, B. Chen, Phys. Rev. D **104**, 024001 (2021). https://doi.org/10.1103/PhysRevD.104.024001
62. S. Vagnozzi, L. Visinelli, Res. Notes AAS **6**, 106 (2022). https://doi.org/10.3847/2515-5172/ac7331
63. I. Banerjee, S. Chakraborty, S. SenGupta, Phys. Rev. D **106**, 084051 (2022). https://doi.org/10.1103/PhysRevD.106.084051
64. I. Sengo, P.V. Cunha, C.A. Herdeiro, E. Radu, J. Cosmol. Astropart. Phys. (2023). https://doi.org/10.1088/1475-7516/2023/01/047
65. S. Vagnozzi, R. Roy, Y.-D. Tsai, L. Visinelli, M. Afrin, A. Allahyari, P. Bambhaniya, D. Dey, S.G. Ghosh, P.S. Joshi, K. Jusufi, M. Khodadi, R.K. Walia, A. Övgün, C. Bambi, Class. Quantum Gravity **40**, 165007 (2023). https://doi.org/10.1088/1361-6382/acd97b
66. F. Atamurotov, F. Sarikulov, S.G. Ghosh, G. Mustafa, Phys. Dark Univ. **46**, 101625 (2024). https://doi.org/10.1016/j.dark.2024.101625
67. E.H.T. Collaboration, Astrophys. J. Lett. **910**, L13 (2021). https://doi.org/10.3847/2041-8213/abe4de
68. R.A. Breuer, J. Ehlers, R. Penrose, Proc. R. Soc. Lond. A Math. Phys. Sci. **370**, 389 (1980). https://doi.org/10.1098/rspa.1980.0040
69. R.A. Breuer, J. Ehlers, R. Penrose, Proc. R. Soc. Lond. A Math. Phys. Sci. **374**, 65 (1981). https://doi.org/10.1098/rspa.1981.0011
70. V. Perlick, O.Y. Tsupko, Phys. Rev. D **95**, 104003 (2017). https://doi.org/10.1103/PhysRevD.95.104003
71. V. Perlick, O.Y. Tsupko, G.S. Bisnovatyi-Kogan, Phys. Rev. D **92**, 104031 (2015). https://doi.org/10.1103/PhysRevD.92.104031
72. A. Chowdhuri, A. Bhattacharyya, Phys. Rev. D **104**, 064039 (2021). https://doi.org/10.1103/PhysRevD.104.064039
73. Z. Zhang, H. Yan, M. Guo, B. Chen, Phys. Rev. D **107**, 024027 (2023). https://doi.org/10.1103/PhysRevD.107.024027
74. G. Briozzo, E. Gallo, T. Mädler, Phys. Rev. D **107**, 124004 (2023). https://doi.org/10.1103/PhysRevD.107.124004
75. F. Atamurotov, B. Ahmedov, A. Abdujabbarov, Phys. Rev. D **92**, 084005 (2015). https://doi.org/10.1103/PhysRevD.92.084005
76. A. Das, A. Saha, S. Gangopadhyay, Class. Quantum Gravity **39**, 075005 (2022). https://doi.org/10.1088/1361-6382/ac50ed
77. M.A. Raza, M. Zubair, E. Maqsood, J. Cosmol. Astropart. Phys. (2024). https://doi.org/10.1088/1475-7516/2024/05/047
78. F. Fazzini, Phys. Rev. D **111**, 046025 (2025). https://doi.org/10.1103/PhysRevD.111.046025
79. H. Ali, S.U. Islam, S.G. Ghosh, arXiv e-prints (2024). https://doi.org/10.48550/arXiv.2410.09198. arXiv:2410.09198 [gr-qc]
80. A. Vachher, S.G. Ghosh, arXiv e-prints (2024). https://doi.org/10.48550/arXiv.2410.11332. arXiv:2410.11332 [gr-qc]
81. J.R. Oppenheimer, H. Snyder, Phys. Rev. **56**, 455 (1939). https://doi.org/10.1103/PhysRev.56.455
82. R.W. Smith, J. Hist. Astron. **29**, 86 (1998). https://doi.org/10.1177/002182869802900108
83. J. Yang, Y. Ding, Y. Ma, Phys. Lett. B **682**, 1 (2009). https://doi.org/10.1016/j.physletb.2009.10.072
84. M. Assanioussi, A. Dapor, K. Liegener, T. Pawłowski, Phys. Rev. Lett. **121**, 081303 (2018). https://doi.org/10.1103/PhysRevLett.121.081303
85. K.A. Meissner, Class. Quantum Gravity **21**, 5245 (2004). https://doi.org/10.1088/0264-9381/21/22/015
86. M. Domagala, J. Lewandowski, Class. Quantum Gravity **21**, 5233 (2004). https://doi.org/10.1088/0264-9381/21/22/014
87. L. Zhao, M. Tang, Z. Xu, Eur. Phys. J. C **84**, 971 (2024). https://doi.org/10.1140/epjc/s10052-024-13342-z
88. S. Luo, arXiv e-prints (2024). https://doi.org/10.48550/arXiv.2409.16323. arXiv:2409.16323 [gr-qc]
89. C. Zhang, J. Lewandowski, Y. Ma, J. Yang, Phys. Rev. D **111**, L081504 (2025). https://doi.org/10.1103/PhysRevD.111.L081504
90. C. Zhang, J. Lewandowski, Y. Ma, J. Yang, arXiv e-prints (2024). https://doi.org/10.48550/arXiv.2412.02487. arXiv:2412.02487 [gr-qc]
91. M. Han, H. Liu, Phys. Rev. D **109**, 084033 (2024). https://doi.org/10.1103/PhysRevD.109.084033
92. M. Bojowald, E.I. Duque, Phys. Rev. D **109**, 084044 (2024). https://doi.org/10.1103/PhysRevD.109.084044
93. J.L. Synge, Mon. Not. R. Astron. Soc. **131**, 463 (1966). https://doi.org/10.1093/mnras/131.3.463
94. S. Chandrasekhar, *The Mathematical Theory of Black Holes*, Vol. 69 (Oxford University Press, Oxford, 1998)
95. B. Carter, Phys. Rev. **174**, 1559 (1968). https://doi.org/10.1103/PhysRev.174.1559
96. K. Hioki, K.-I. Maeda, Phys. Rev. D **80**, 024042 (2009). https://doi.org/10.1103/PhysRevD.80.024042. arXiv:0904.3575 [astro-ph.HE]
97. A.A. Abdujabbarov, L. Rezzolla, B.J. Ahmedov, Mon. Not. R. Astron. Soc. **454**, 2423 (2015). https://doi.org/10.1093/mnras/stv2079. arXiv:1503.09054 [gr-qc]
98. R. Kumar, S.G. Ghosh, Astrophys. J. **892**, 78 (2020). https://doi.org/10.3847/1538-4357/ab77b0
99. R. Kumar, S.G. Ghosh, J. Cosmol. Astropart. Phys. (2020). https://doi.org/10.1088/1475-7516/2020/07/053
100. E.H.T. Collaboration, Astrophys. J. Lett. **875**, L5 (2019). https://doi.org/10.3847/2041-8213/ab0f43
101. E.H.T. Collaboration, Astrophys. J. Lett. **875**, L6 (2019). https://doi.org/10.3847/2041-8213/ab1141
102. E.H.T. Collaboration, Astrophys. J. Lett. **930**, L12 (2022). https://doi.org/10.3847/2041-8213/ac6674
103. E.H.T. Collaboration, Astrophys. J. Lett. **930**, L17 (2022). https://doi.org/10.3847/2041-8213/ac6756